Journal of Trace Elements in Medicine and Biology 54 (2019) 8–20

Contents lists available at ScienceDirect

Journal of Trace Elements in Medicine and Biology

journal homepage: www.elsevier.com/locate/jtemb

Bioinorganic chemistry

Enhanced antibacterial activity of hemocyanin purified from *Portunus pelagicus* hemolymph combined with silver nanoparticles – Intracellular uptake and mode of action

Ramachandran Ishwarya[a], Baskaralingam Vaseeharan[a,*], Sivakumar Shanthini[b], Marimuthu Govindarajan[c,d], Naiyf S. Alharbi[e,*], Shine Kadaikunnan[e], Jamal M. Khaled[e], Mohammed N. Al-anbr[e]

[a] *Crustacean Molecular Biology and Genomics Division, Biomaterials and Biotechnology in Animal Health Lab, Department of Animal Health and Management, Alagappa University, Science Block, 6th floor, Burma Colony, Karaikudi, 630 004, Tamil Nadu, India*
[b] *Centre for Animal Science Research and Extension Services, Foundation for Innovative Research in Science and Technology, Kelavannanvilai, NGO Colony Road, Nagercoil, Tamil Nadu, India*
[c] *Unit of Vector Control, Phytochemistry and Nanotechnology, Department of Zoology, Annamalai University, Annamalainagar, Tamil Nadu, 608 002, India*
[d] *Department of Zoology, Government College for Women, Kumbakonam, 612 001, Tamil Nadu, India*
[e] *Department of Botany and Microbiology, College of Science, King Saud University, Riyadh, 11451, Saudi Arabia*

ARTICLE INFO

Keywords:
Bacterial biofilm
DNA fragmentation
Reactive oxygen species
Malondialdehyde
Membrane damage
Nucleic acid leakage
Peroxidase
Superoxide dismutase

ABSTRACT

Recently, biogenic nanoparticles have been considered promising candidates for manufacturing antibacterial nanodrugs. Here, we synthesized AgNPs using the crab-borne antibacterial agent hemocyanin and assessed the antibacterial action against several pathogenic bacteria. In this study, the crustacean immune protein hemocyanin (*Pp*-Hc, 78 kDa) purified from *Portunus pelagicus* hemolymph was used to fabricate silver nanoparticles. Characterization of hemocyanin-fabricated AgNPs (*Pp*-Hc AgNPs) were achieved using ultraviolet-visible spectrophotometer, X-ray powder diffraction (XRD), Fourier-transform infrared spectroscopy (FTIR), high-resolution-transmission electron microscopy (HR-TEM), and energy-dispersive X-ray spectroscopy. The antibacterial efficacy of $AgNO_3$, *Pp*-Hc and *Pp*-Hc AgNPs was compared by growth inhibition, antibiofilm and live and dead analyses. Based on the results, *Pp*-Hc AgNPs was more efficient than *Pp*-Hc and $AgNO_3$ against pathogenic bacteria. Mechanistic analysis revealed membrane damage and reactive oxygen species (ROS) generation, suggesting that *Pp*-Hc and *Pp*-Hc AgNPs rely to similar modes of action. Intracellular protein molecules and nucleic acid leakage confirmed that *Pp*-Hc AgNPs increase membrane permeability, leading to cell death. Based on our results, capping of the exterior surface of nanoparticles with antimicrobial crab-borne peptides, such as *Pp*-Hc, improves their functions as potential agents against bacterial diseases, which may be useful in clinical applications.

1. Introduction

Antibiotics are highly important in the fight against bacterial infections, to reduce the morbidity and mortality of humans, as well as in livestock and pets worldwide. However, in the past few years, an increase in antibiotic resistance of microorganisms – largely due to the overuse of antibiotics – has become a severe problem worldwide [1–3]. An approach for overcoming this problem is to use novel, low-cost, and efficient antimicrobial agents that have biological ability to reduce the rate and spread of resistance development of target microorganisms [4,5]. An increased incidence of infections caused by antibiotic-resistant microbial strains expanded the attention about antimicrobial properties of silver and its composites [6,7]. Silver has been used as an antimicrobial complex since before the beginning of antibiotics in the 1940s, and is currently used in a broad array of medicinal purposes because of its antibacterial effects and relatively small toxicity to human cells [8–10]. However, the cost burden and current identification of silver-resistant bacteria pointed out the inadequate use of raw silver as possible alternative to broad-spectrum antibiotics [11].

Nanotechnology has rapidly advanced in the current century because of the stunning potential of nanomaterials, with special reference to nanosize, which radically modifies their physical, chemical, and

* Corresponding authors.
E-mail addresses: vaseeharanb@gmail.com (B. Vaseeharan), nalharbi1@ksu.edu.sa (N.S. Alharbi).

https://doi.org/10.1016/j.jtemb.2019.03.005
Received 27 September 2018; Received in revised form 6 March 2019; Accepted 9 March 2019

optical properties [12–20]. Metal nanoparticles are promising as antimicrobials and antiparasitic drugs and show potential for large-scale commercialization [21–28]. It has been suggested that, the metallic silver nanoparticles (AgNPs) have an antimicrobial activity against several pathogenic microorganisms. Nanosilver functions as a disinfectant that can considerably decrease several bacterial diseases for a long period of time compared to general biocides, such as tetracycline and penicillin. The mechanisms leading to the antimicrobial properties of AgNPs are not entirely understood. Probably, as noted for the mechanisms of action of Ag^+ ions, they involve morphological modifications in bacterial cells as well as in several invertebrate species. Although numerous researches have established the antimicrobial properties of AgNPs [29], few studies have examined the mechanisms triggered by AgNPs to achieve their antimicrobial activity. For bacteria, generally proposed mechanisms include the discharge of Ag^+ ions [30,31], which induce reactive oxygen species (ROS) generation [32] and malfunction of the microbial cell membrane [33]. However, several conflicting findings have been reported.

Many biological methods can be used to fabricate AgNPs and other metal and metal oxide NPs using extracts or metabolites from various organisms as reducing and capping agents [34–42]. A major role has been reported for polysaccharides, proteins, amino acids and vitamins [43–45]. Hemocyanins are copper-containing immune molecules present in the hemolymph of crustaceans. They direct the transport of oxygen in innate immune responses, showing phenoloxidase-like activity [46]. Hemocyanins are a source of wide-ranging antimicrobial peptides in crustaceans. Previously, Jayanthi et al. [47] described the synthesis of AgNPs covered with lectin purified from *Portunus pelagicus* and assessed their antibacterial and antibiofilm activities. A similar trend was noted analyzing β-glucan-binding protein from *P. pelagicus* and *Paratelphusa hydrodromus*-coated silver and zinc nanoparticles, respectively [48,49]. Additionally, the antibacterial activity of protein-capped AgNPs has been reported by Chowdhury et al. [50] and Jain et al. [51].

The present work, we evaluated *P. pelagicus* hemocyanin (*Pp*-Hc)-mediated synthesis and capping of AgNPs relying to a biological approach. We assessed the antibacterial and antibiofilm effects of $AgNO_3$, purified *Pp*-Hc and synthesized *Pp*-Hc AgNPs against *Enterococcus faecalis* (Gram positive bacterium) and *Shigella sonnei* (Gram-negative bacterium). Additionally, assays to shed light on their mode of action were carried out, assessing membrane damage and reactive oxygen species generation (ROS) triggered via $AgNO_3$, *Pp*-Hc and *Pp*-Hc AgNPs exposure. Intracellular protein and nucleic acid leakage experiments were also investigated.

2. Materials and methods

2.1. Animals

Animal testing was done using blue swimmer crabs collected from Mandapam, Ramnad District, Tamil Nadu, India located between 9.2770 °N latitude 79.1252 °E longitude and placed in large fiber reinforced plastic (FRP) containers with 500 L water. Healthy blue swimmer crabs among normal weight of approximately 160 g were stocked for three days and feed daily at 10% of body weight through diet (sliced fish plus shrimp meat).

2.2. Purification of hemocyanin

Hemocyanin was purified from blue swimmer crabs as described by Ishwarya et al. [52]. Hemolymph was collected from the right chelate leg with a hygienic syringe. An equal amount of anticoagulant solution was present in the syringe to prevent coagulation of the hemolymph. The collected hemolymph was centrifuged at 800 ×*g*, refrigerated at 4 °C, for 10 min then the supernatant liquid was removed and immediately submitted to gel filtration chromatography at 4 °C. Next, Tris-buffered saline (TBS; 20 mL) was mixed with the supernatant and passed over a Sephadex G-100 column that had been pre-equilibrated with TBS/$CaCl_2$ buffer. Proteins were eluted through rinsing the column by TBS and then dialyzed for 24 h.

2.3. SDS-PAGE

To separate the hemocyanin according to its electrophoretic mobility, a sodium dodecyl sulfate-polyacrylamide gel electrophoresis (SDS-PAGE) was carried out (12% separating and 4% stacking gel) as reported by Ishwarya et al. [46]. The hemocyanin molecular weight was determined by comparison with a protein marker (Himedia Laboratories, Karnataka, India).

2.4. Production and characterization of Pp-Hc AgNPs

A silver nitrate (1 mM) was vigorously mixed with 50 mL of double-distilled water using a magnetic mixer. Following the dissolution of the reaction mixture, Pp-Hc (5 mL) was added and mixed for 3 h using the magnetic stirrer at room temperature. The reaction solution was placed in the dark until observation the reddish brown color in the reaction mixture. Then, the centrifugation of the reaction solution was performed at 5000 ×g for 15 min and the pellets were collected after throwing the supernatant away and the collected pellets were dried using the desiccator. The obtained *Pp*-Hc AgNPs were characterized. UV spectrum scanning was carried out on the *Pp*-Hc AgNPs reaction mixture with UV–vis spectrophotometer (scanning: 200–700 cm^{-1}, resolution: 1 nm). The NP crystalline phase and purity were evaluated by XRD analysis with a X-ray powder diffraction (XRD) (X'Pert Pro, PANalytical, Almelo, The Netherlands) by a ʎ of 1.5406 Å and nickel monochromator. Functional biomolecules in the *Pp*-Hc AgNPs suspension were analyzed by FTIR (Perkin-Elmer, Waltham, MA, USA) spectroscopy (wavelenght: 500–4000 cm^{-1}; resolution: 4 cm^{-1}). To study the morphologic features and size of *Pp*-Hc AgNPs, HR-TEM (TEM-100 keV JEOL 1200, Jeol Ltd., Tokyo, Japan) was conducted, after preliminary SEM studies, using an electrical energy of 200 kV. Lastly, EDX spectroscopy was applied to investigate the chemical composition of *Pp*-Hc AgNPs. The size distribution and stability (zeta potential) of *Pp*-Hc AgNPs were determined using dynamic light scattering (DLS) (Zetasizer Nano ZS, ZEN3600 and Malvern, UK). Measurements were carried out at 25 °C and the synthesized *Pp*-Hc AgNPs (100 µg/ml) were diluted with milliQ water and the diluted sample was permitted to filter throughout 0.22-µm syringe filter and it was transfer to square cuvette for DLS.

2.5. Antibacterial efficiency of Pp-Hc AgNPs

The antibacterial potential of $AgNO_3$, *Pp*-Hc and *Pp*-Hc AgNPs was assessed on Gram-positive, i.e., *E. faecalis* (strain HQ 693279.1) and Gram-negative, i.e., *S. sonnei* (strain K 7769531), bacteria.

2.5.1. Antibacterial activity

Agar well diffusion assay was applied to determine the biological activity of *Pp*-Hc as antibacterial agent. Bacterial culture was uniformly spread using an autoclaved cotton swab on a sterile Luria-Bertani agar (Himedia, India), and wells (7 mm diameter) were punched with a sterile cork-borer. The $AgNO_3$ (100 µg/mL), purified *Pp*-Hc or *Pp*-Hc AgNPs (50 and 100 µg/mL, respectively) was added into the wells and incubating at 35 ± 1 °C for 24 h. Inhibition zone was measured in mm with a ruler from the well to the end of the clear zone.

2.5.2. Minimum inhibitory concentration (MIC) of Pp-Hc AgNPs

To determine the MIC of $AgNO_3$, purified *Pp*-Hc and *Pp*-Hc AgNPs, the susceptibility of *E. faecalis* and *S. sonnei* to the serial dilution concentrations of $AgNO_3$, purified *Pp*-Hc and *Pp*-Hc AgNPs were

determined using serial macrodilution methods according to Luo et al. [53]. The total count of bacteria in the test tubes was 1×10^5 CFU/mL and the serial dilution concentrations of $AgNO_3$, *Pp*-Hc and *Pp*-Hc AgNPs ranged from 10 to 100 μg/mL. The incubation was aerobically done at 35 ± 1 °C for 24 h then the broth (1.5 mL) from all tubes were taken at different time points and turbidity was recorded at a wavelength of OD 600 nm.

2.6. Antibacterial mechanisms

2.6.1. Preparation of bacterial extract and biochemical assays

To prepare the bacterial extract, a test tube containing nutrient broth (5 mL) was exposed to *E. faecalis* and *S. sonnei* (10^8 CFU/mL). Bacteria were challenged with $AgNO_3$ (100 μg/mL), purified *Pp*-Hc and *Pp*-Hc AgNPs (50 and 100 μg/mL, respectively) and incubated for one day. The bacterial cells were centrifuged for 7000 ×*g* at 10 min, the pellet was collected and sonicated to acquire the crude enzyme extract. Bacterial cells not exposed to $AgNO_3$, *Pp*-Hc and *Pp*-Hc AgNPs treatment were used as controls. Peroxidase (POD) activities were calculated in triplicate as described by Hochman and Goldberg et al. [54]. The reaction solution for POD analysis contained 0.01 M pyrogallol (1 mL), 0.1 M phosphate buffer (2 mL; pH 6.0), and 5 mM hydrogen peroxide (1 mL). The assay was started by adding enzyme extract (1 mL) pursued by incubating for room temperature at 5 min. Then, the 2.5 N H_2SO_4 (1 mL) added to stop the reaction and the quantity of purpurogallin produced was determined by calculating the OD at 420 nm (Eliza plate reader, Robonik, India).

Superoxide dismutase (SOD) activity was calculated following Arora et al. [55]. Briefly, the reaction solution having 13.0 mM methionine, 6.3 μM NBT, 6.5 μM riboflavin, 0.1 mM EDTA, and PBS (pH 7.8). The assay started mixing enzyme extract (500 μL) and reaction solution (1.5 mL) followed by incubation for 30 °C at 10 min. Then, the tubes were placed in the shade and absorbance was recorded at 560 nm (Eliza plate reader, Robonik, India).

Malondialdehyde (MDA) formation was detected to assess membrane damage using thiobarbituric acid as described previously Buege et al. [56]. The enzyme extract was hydrated in trichloroacetic acid (1 mL of 2.5% (w/v) and centrifuged for 12,000 ×*g* at 20 min at 4 °C, supernatant (100 μL) was 0.5% (w/v) thiobarbituric acid reagent prepared in 20% (w/v) TCA. The reaction solution was heated on 100 °C in a water bath, and then centrifuged at 12,000 ×*g* at 10 min for 4 °C. Absorbance was recorded at 532 nm (Eliza plate reader, Robonik, India).

Oxidative stress induced by $AgNO_3$ (100 μg/mL), purified *Pp*-Hc and *Pp*-Hc AgNPs (50 and 100 μg/mL, respectively) to the bacterial cells is reflected by ROS production. The effects of $AgNO_3$, *Pp*-Hc and *Pp*-Hc AgNPs on intracellular ROS generation in the bacteria were observed in a 2′,7′-dichlorofluorescein diacetate DCF-DA assay, which was conducted using a regular procedure [57]. In brief, the bacterial cells (10^8 CFU/mL) were harvested via centrifugation, rinsed two times with PBS, and incubate with 10 μM DCF-DA in PBS at room temperature for 30 min. The $AgNO_3$, purified *PP*-Hc and *Pp*-Hc AgNPs with the cells were incubating for room temperature at one day. Intracellular ROS level was determined through confocal laser scanning microscopy (CLSM) (Carl Zeiss; LSM 710, Oberkochen, Germany).

2.7. Leakage of intracellular molecules

We next examined whether cell membrane permeability was altered by the $AgNO_3$ (100 μg/mL), purified *Pp*-Hc and *Pp*-Hc AgNPs (100 and 50 μg/mL, respectively). Leakages of intracellular molecules by treated bacterial cells was studied using the fluorescent dyes fluorescein isothiocyanate (FITC) and propidium iodide (PI), which cannot cross the membrane and is expelled from viable cells. The $AgNO_3$ (100 μg/mL), Purified *Pp*-Hc and *Pp*-Hc AgNPs-treated bacterial cells were centrifuged at 8500 ×*g* for 5 min at 4 °C and the supernatant was varied with FITC and PI for 20 min incubation at room temperature in the dark. Leakage of intracellular molecules was observed using CLSM.

2.8. DNA fragmentation assay

The DNA fragmentation assay was carried out according to the protocol by Datkhile et al. [58] with slight modifications. Briefly, bacterial samples were treated with $AgNO_3$ (100 μg/mL), purified *Pp*-Hc and *Pp*-Hc AgNPs (50 and 100 μg/mL, respectively) incubate for 24 h. Then, DNA was extracted from the control bacterial samples and treated samples. DNA extraction method was published earlier [59], with slight changes. Following purification, extracted DNA samples were separated in an agarose gel and analyzed for any changes. DNA fragments were visualized with a UV trans-illuminator and photographs were acquired with a gel documentation system (Progen, G- Doc system, Mumbai).

2.9. Microscopic biofilm observation

The bacterial culture in LB broth was diluted to an OD of 0.5 (OD 600). Culture (1 mL) aliquots were added to a microtiter plate (24 well) containing glass pieces (13 × 13 mm) in presence and absence of $AgNO_3$ (100 μg/mL), *Pp*-Hc and *Pp*-Hc AgNPs (50 and 100 μg/mL, respectively), and then incubating at room temperature for 16 h. The glass pieces were washed thoroughly by 0.01 M PBS. Glass pieces were moved from the slides and crystal violet dye (0.4%) was used for staining, followed by light microscopy visualization (40×). Morphological observation of the biofilm was also carried out by SEM analysis after that biofilms were Au-coated with a sputter coater and images were acquired. Besides, biofilms produced on cover glasses in presence or not of $AgNO_3$ (100 μg/mL), *Pp*-Hc and *Pp*-Hc AgNPs were stained by solution of acridine orange (0.4% w/v) for 10 min and images were acquired by CLSM.

2.10. Live/dead bacterial (Baclight) assay

The Live/Dead Baclight L-7012 kit (Invitrogen, Carlsbad, CA, USA) was used to analyze the live and adhered bacterial cells by confocal microscopy. The bacterial strains (10^6 CFU/mL) were treated with the MIC concentrations of $AgNO_3$ (100 μg/mL), purified *Pp*-Hc and *Pp*-Hc AgNPs (50 and 100 μg/mL, respectively) and incubated for 60 min. The cells were centrifuged for 6000 ×*g* at 5 min at 4 °C and the pellet was rinsed with PBS. The cells were stained with SYTO 9 and PI for 15 min in the dark and images were acquired by CLSM.

2.11. Dissolution of Pp-Hc -AgNPs

The dissolution of *Pp*-Hc AgNPs was prepared via dispersing *Pp*-Hc AgNPs in distilled water with a bath sonicator for 30 min to split amassed as much as potential. To establish whether Ag^+ dissolved from *Pp*-Hc AgNPs suspensions may play a part in the observed bactericidal activity, *Pp*-Hc AgNPs (20–100 μg L^{-1}) was centrifuge for 8000 *g* at 20 min and clear supernatants were cautiously collected. The released Ag^+ concentration in the supernatants were measured by iCE 3000 series, Graphite tube atomizer, Atomic Absorption Spectrometer (Thermo Scientific).The Merck silver nitrate is used for standarad.

2.12. Statistical data analysis

Every assay was conducted in three replicates and the final values were mean ± standard deviation (SD). Two-way ANOVA and Tukey's HSD test were used to assess significant differences among treatments and tested bacterial species. P-values < 0.05 were considered as statistically significant.

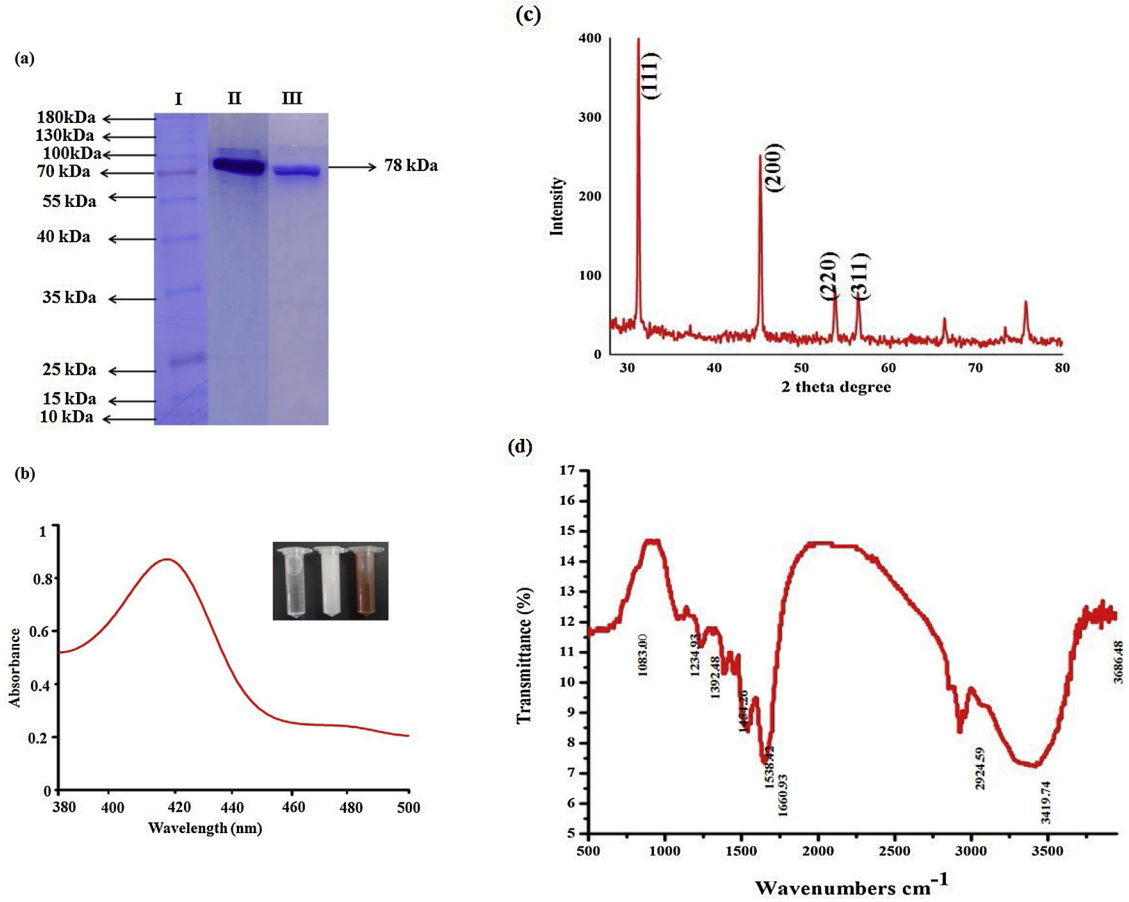

Fig. 1. SDS-PAGE analysis of *Portunus pelagicus* hemocyanin (*Pp*-Hc) capping the silver nanoparticles (AgNPs) tested in this study. Lane I: molecular size marker. Lane II: *Pp*-Hc. Lane III: *Pp*-Hc AgNPs showing the 78-kDa capping protein (a). UV–vis spectroscopy of *Portunus pelagicus* hemocyanin-synthesized Ag nanoparticles (*Pp*-Hc AgNPs) (b), X-ray diffraction (XRD) analysis and (c), FT-IR spectrum of *Pp*-Hc AgNPs (d).

3. Results and discussion

3.1. Purification of hemocyanin

Pp-Hc was purified from the hemolymph of *P. pelagicus* by gel filtration chromatography. The purity and molecular mass of *Pp*-Hc was investigated by gel electrophoresis. Fig. 1a confirms a distinct band of about 78 kDa in 12% SDS-PAGE below reducing conditions. Following the production of AgNPs, a reaction can be conducted to stabilize the nanoparticles using capping agents (protein). To characterize the purified hemocyanin associated with AgNPs, SDS-PAGE was conducted. AgNPs were mixed with SDS and boiled in a water bath for 10 min. The boiled sample displayed a strong band at 78 kDa (Fig. 1a, lane II), which ran at the same molecular weight of the protein band in the hemolymph of *P. pelagicus* (Fig. 1a, lane III). This 78-kDa Hc can act as capping material stabilizing AgNPs. Indeed, proteins in the hemolymph of crustaceans are responsible for synthesis and stability of AgNPs as described previously [47–50].

3.2. Characterization of Pp-Hc AgNPs

The reduction of Ag^+ ions from $AgNO_3$ to *Pp*-Hc AgNPs was primarily observed as a colorless solution changing to reddish-brown, which indicated the synthesis of *Pp*-Hc AgNPs. AgNPs were subjected to UV–vis spectroscopy analysis. The absorption spectrum of AgNPs displayed single-band absorption, with a peak at 420 nm (Fig. 1b). This specifies the occurrence of AgNPs, displaying the longitudinal excitation of surface plasmon resonance (SPR), a distinctive characteristic of AgNPs [60]. Because of the crystalline nature of AgNPs, XRD peaks appeared at (111), (200), (220), and (311) for Ag at 2Θ angles of 31.2, 45.2, 66.5, and 76.6, respectively (Fig. 1c). XRD analysis results were evaluated based on the Joint Committee on Powder Diffraction standards (JCPDS 01-1167). Comparing our XRD spectrum with standard data, it has been noted that nanosilver formed in our research had the appearance of nanocrystals [61]. A comparable pattern in the XRD spectrum has been described for AgNPs synthesized by different proteins such as lectin [47] and β-glucan-binding protein [48].

The *Pp*-Hc AgNPs were examined by FTIR spectroscopy (Fig. 1d). The FTIR spectrum showed peaks at 3686.48, 3419.74, 2924.59, 1660.93, 1538.42, 1454.26, 1380.48, 1234.93, and 1030.00 cm^{-1}. The band at 1600–1700 cm^{-1} named as amide I was associated with C═O stretching vibration of the backbone conformation [62]. The bonds at 2920–2950 cm^{-1} correspond to C−H groups [63], whereas bands at 1620–1650 cm^{-1} are recognized as –C (O)– of peptide bonds and/or $–NH_2$ groups, and those at 1380–1030 cm^{-1} reflected CN bonds [64,65]. Along with the FTIR results, the protein-capped nanosilver surface did not show related secondary structure modifications by interacting with AgNPs, nor while covalently bonded as described previously. The interaction among the proteins and AgNPs may be covalent binding to cysteine residues and amino groups and electrostatic communication may occur through carboxyl groups [66].

3.3. Morphological analysis of Pp-Hc AgNPs

TEM revealed that the synthesized *Pp*-Hc AgNPs are spherical and cubic shaped. (Fig. 2a). Fig. 2b shows the selected area diffraction pattern of *Pp*-Hc AgNPs, illustrating that the particles are well-crystallized and the occurrence of ring outline in the distinct face centered

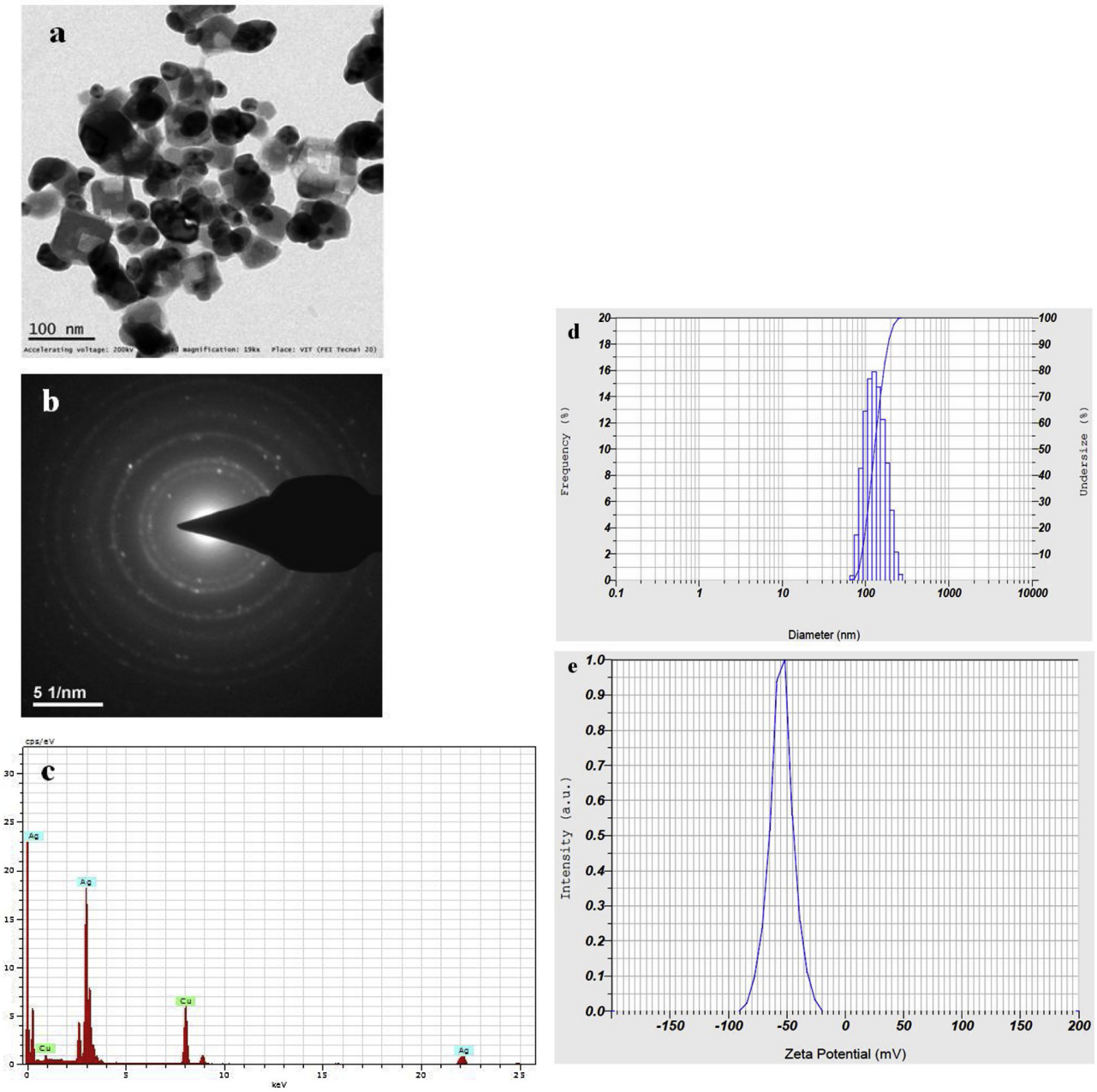

Fig. 2. TEM (a) showing size and surface morphology of *Pp*-Hc AgNPs, (b) SAED pattern, (c) EDX spectrum, (d) DLS and (e) Zeta potential.

cubic crystalline nature of AgNPs. In Fig. 2c, a standard EDX spectrum is shown. The spectrum showed five peaks between 2 and 8 kV. The maxima were associated with the Ag-distinctive lines. Quantitative analysis confirmed high silver contents (75%) in the samples. Our *Pp*-Hc AgNPs are small and poly-dispersed in nature. These features are important for antibacterial properties, as they can cross the bacterial cell membrane to disrupt the respiratory chain, DNA, RNA, and cell metabolism, finally resulting in cell death [67].

The particle size distribution image of *Pp*-Hc AgNPs shown in Fig. 2d. It is observed that the size distribution of *Pp*-Hc AgNPs ranges from 70 to 200 nm and the calculated average size distribution is 134 nm. The zeta potential of *Pp*-Hc AgNPs was found as a sharp peak at -54.5 mV (Fig. 2e). It is recommended that the surface of the nanoparticles is negatively charged and dispersed in the medium. The negative value proves the repulsion between the particles and confirms that they are very stable.

3.4. Antibacterial efficiency of purified Pp-Hc and Pp-Hc AgNPs

In vitro antibacterial activity of $AgNO_3$, *Pp*-Hc and *Pp*-Hc AgNPs was determined by the well diffusion assay. The zone of inhibition appeared around the wells loaded with purified $AgNO_3$, *Pp*-Hc and *Pp*-Hc AgNPs, demonstrating that *Pp*-Hc AgNPs had a strong antimicrobial effect ($P < 0.05$) (Fig. 3a).

Experiments conducted here were aimed to establish the MIC of $AgNO_3$, *Pp*-Hc and *Pp*-Hc AgNPs on bacterial pathogens Gram-positive (*E. faecalis*) and Gram-negative (*S. sonnei*). Results showed that *Pp*-Hc AgNPs exhibited considerable inhibitory effects towards *E. faecalis* and *S. sonnei* than *Pp*-Hc and $AgNO_3$. The $AgNO_3$, *Pp*-Hc and *Pp*-Hc AgNPs, showed a significant effect of the tested concentration ($F_{4,10} = 131.100$, $P < 0.0001$; $F_{4,20} = 122.421$, $P < 0.0001$; $F_{4,20} = 65.990$, $P < 0.0001$ respectively) and the bacterial species was observed ($F_{4,10} = 60.913$, $P < 0.0001$; $F_{1,20} = 35.579$, $P < 0.0001$; $F_{4,20} = 7.558$, $P = 0.012$ respectively). The interaction

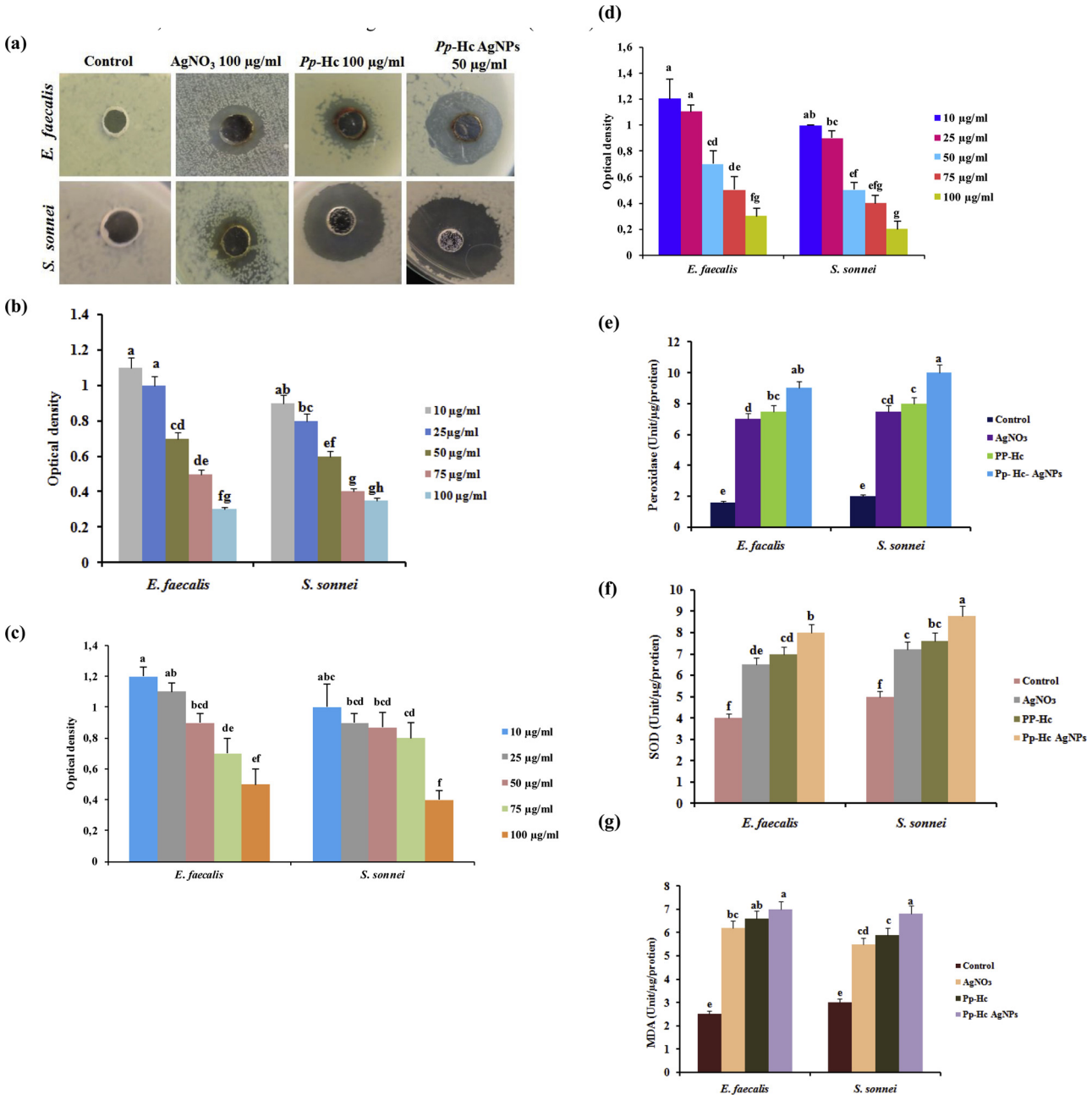

Fig. 3. Zones of inhibition post-treatment with $AgNO_3$, *Pp*-Hc and *Pp*-Hc AgNPs (a). Inhibitory effects of $AgNO_3$ (b), *Pp*-Hc (c) and *Pp*-Hc AgNPs (d). T-bars represent standard deviations. Above each column, different letters indicate significant differences ($P < 0.05$). Levels of peroxidase (e) and superoxide dismutase (SOD) (f) in untreated and treated bacterial cells. Malondialdehyde (MDA) assay showing the difference in membrane damage capability post-treatment with $AgNO_3$, *Pp*-Hc, and *Pp*-Hc AgNPs (g). T-bars represent standard deviations. Above each column, different letters indicate significant differences ($P < 0.05$).

species*concentration was significant testing *Pp*-Hc AgNPs ($F_{1,20} = 4.279$, $P = 0.012$), while no significant differences were detected in *Pp*-Hc assays ($F_{4,20} = 0.842$, $P = 0.542$). Significant inhibition of bacterial pathogen growth was observed at concentrations of 10 and 100 µg/mL of $AgNO_3$, *Pp*-Hc and *Pp*-Hc AgNPs, over the control ($P < 0.05$) (Fig. 3b–d). The value gradually decreased with increasing nanoparticle exposure to the bacteria. However, 10, 50, and 100 of µg/mL of $AgNO_3$, *Pp*-Hc and *Pp*-Hc AgNPs showed no significant differences in cell density. Therefore, 100 µg/mL of $AgNO_3$, *Pp*-Hc and 50 µg/mL of *Pp*-Hc AgNPs were considered as the highest MICs and these three concentrations were used as standards for the antibacterial and anti-biofilm assays.

3.5. Bactericidal mechanism of purified Pp-Hc and Pp-Hc AgNPs

In practical applications, small rather than large AgNPs are utilized because they are highly toxic and a low dosage can kill bacteria. Nanoparticle-induced induction of cytotoxicity was measured as the initiation of ROS production [68]. The function of ROS generation and its consequences on the antioxidant system were assessed determining the activity of ROS-associated enzymes such as peroxidase (POD) (Fig. 3e) and superoxide dismutase (SOD) (Fig. 3f). Enhanced activities of both enzymes were showed in the tested bacterial species following the exposure to $AgNO_3$, *Pp*-Hc and *Pp*-Hc AgNPs. Significant differences were detected according to the treatment (POD: $F_{2,12} = 259.646$, $P < 0.0001$; SOD: $F_{2,12} = 150.150$, $P < 0.0001$; MDA: $F_{2,12} = 135.151$, $P < 0.0001$) and the tested bacterial species (POD:

$F_{1,12} = 7.457$, $P = 0.018$; SOD: $F_{1,12} = 24.091$, $P < 0.0001$; MDA: $F_{1,12} = 1.198$, $P = 0.295$). The interaction treatment*bacterial species was never significant (POD: $F_{2,12} = 0.370$, $P = 0.698$; SOD: $F_{2,12} = 0.364$, $P = 0.702$; MDA: $F_{2,12} = 1.354$, $P = 0.295$) (Fig. 3e–g).

Notably, decreased glutathione levels, enhanced ROS levels, and lipid peroxidation due to *in vivo* contact with AgNPs, have been previously described [69]. The formation of free radicals including superoxide, peroxide, and hydroxyl ions post-exposure to AgNPs has been described to involve lipid peroxidation and disrupt membrane integrity [70–73].

Moreover, biochemical and proteomic studies revealed that AgNPs resulted in instant dissolution of the proton motive force, which causes de energization of the cell membrane and leads to cell death [74]. A membrane damage assay was conducted by determining the MDA content. Generally, an enlarged MDA content was showed in tested bacterial pathogens while showing to $AgNO_3$, *Pp*-Hc and *Pp*-Hc AgNPs (Fig. 3g). In contrast, only a minor difference was observed between *Pp*-Hc and *Pp*-Hc AgNPs ($P < 0.05$).

3.6. Bacterial viability assay

To evaluate bacterial survival after purified $AgNO_3$, *Pp*-Hc and *Pp*-Hc AgNPs exposure at different concentrations, fluorescent dye-based live and dead assays for *E. faecalis* and *S. sonnei* were conducted. Bacteria without the addition of purified $AgNO_3$, *Pp*-Hc and *Pp*-Hc AgNPs served as controls. Bacterial cells without *Pp*-Hc AgNPs exposure showed a green fluorescent color, demonstrating that the control cells were viable (Fig. 4). The *E. faecalis* and *S. sonnei* strains were mixed with the bactericidal concentrations of $AgNO_3$ (100 µg/mL) *Pp*-Hc and *Pp*-Hc AgNPs (100 µg/mL and 50 µg/mL) showed green (live) and red (dead) fluorescent color (Fig. 4b–d). Conversely, $AgNO_3$, *Pp*-Hc and *Pp*-Hc AgNPs treated bacteria confirmed that the greater quantity of dead bacterial cells, that indicating an efficient bactericidal property of *Pp*-Hc AgNPs than *Pp*-Hc and $AgNO_3$. Approximately all bacterial cells died following treatment with AgNPs, revealing strong bactericidal activity [75,76].

3.7. Characterization of bacterial cell damage

Concerning antibacterial mechanisms, it was observed that cellular functional modifications of bacteria after treatment with $AgNO_3$, purified *Pp*-Hc and *Pp*-Hc AgNPs resulted in oxidative stress. Free radicals produced because of AgNPs cause relevant injuries of the bacterial cell membrane. High levels of ROS boost oxidative stress in the cells and cause damage to protein, nucleic acids, and the respiratory chain [77]. In the current study, DCF-DA was used as an intracellular ROS indicator in treated cells. After exposure to $AgNO_3$,purified *Pp*-Hc and *Pp*-Hc AgNPs for 1 h, bacteria were stained with DCFH-DA for 60 min. AgNP-treated bacteria produced DCF^+ (Fig. 5a), with green fluorescent cells indicating that ROS were fabricated resulting in *Pp*-Hc AgNP-induced cell death. Control cells not exposed to nanoparticles did not show DCF^+ green fluorescent staining and appeared black. Bacterial inhibition occurs largely because of the ROS generated when bacterial solutions contact foreign particles [78].

Overproduction of ROS leads to oxidative stress, causing harm to proteins, lipids, and nucleotides, which modify physiological functions [79]. Based on the above findings, the antibacterial activity of purified $AgNO_3$, *Pp*-Hc and *Pp*-Hc AgNPs occurred by disrupting the bacterial membrane and producing intracellular ROS. In our study, the ROS generation and bacterial cell damage was moderately superior in bacterial cells which exposed to *Pp*-Hc AgNPs than *Pp*-Hc and $AgNO_3$.

3.8. Release of intracellular proteins – FITC

To support the above results, we examined the discharge of biomolecules (i.e., proteins and nucleic acid) from bacterial cells following AgNP-based treatment. Remarkably, $AgNO_3$, purified *Pp*-Hc and *Pp*-Hc AgNPs promoted bacterial membrane injury and release of amino acids from cells, as observed by FITC staining. The $AgNO_3$, purified *Pp*-Hc and *Pp*-Hc AgNP-treated *E. faecalis* and *S. sonnei* supernatants were stained with FITC-I and spots were visualized by CLSM. The green spots revealed (Fig. 5b) that the treated bacterial cells released amino acids. Green spots were not showed in the control sample, indicating viable bacterial cells. The release of intracellular proteins by AgNP-treated bacteria was comparable to the results of an earlier study [56].

To further examine whether the permeability of $AgNO_3$, purified *Pp*-

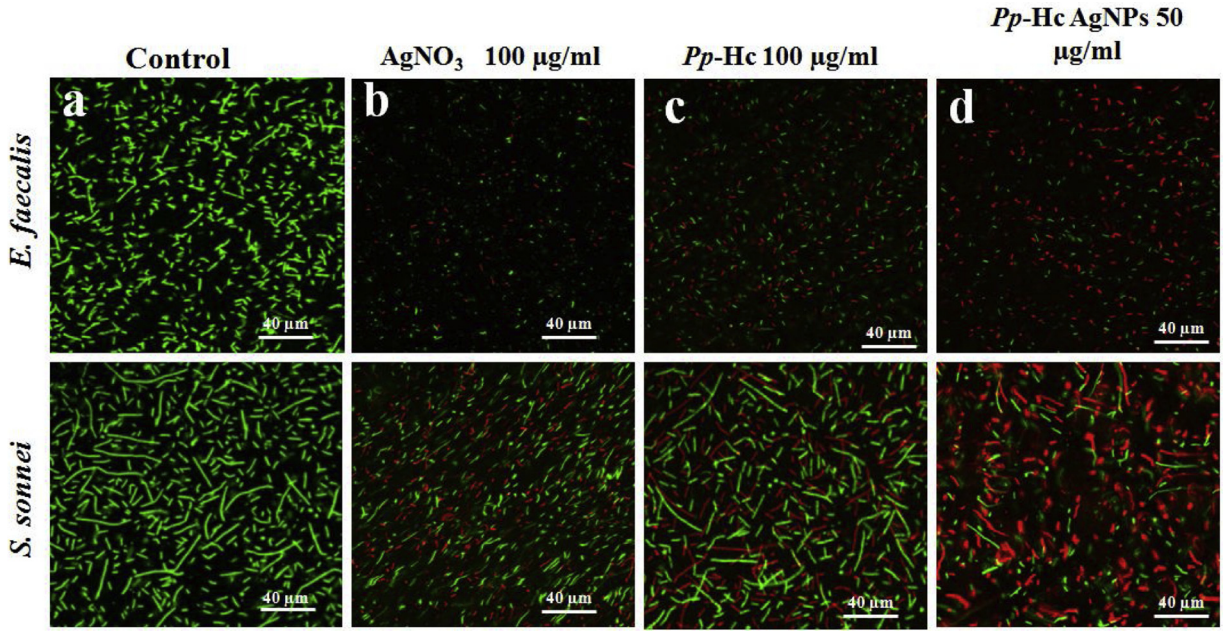

Fig. 4. Laser confocal images of live (green) and dead (red) Gram positive (*E. faecalis*) and Gram negative (*S. sonnei*) bacteria before and after treated with $AgNO_3$, *Pp*-Hc and *Pp*-Hc AgNPs (For interpretation of the references to colour in this figure legend, the reader is referred to the web version of this article).

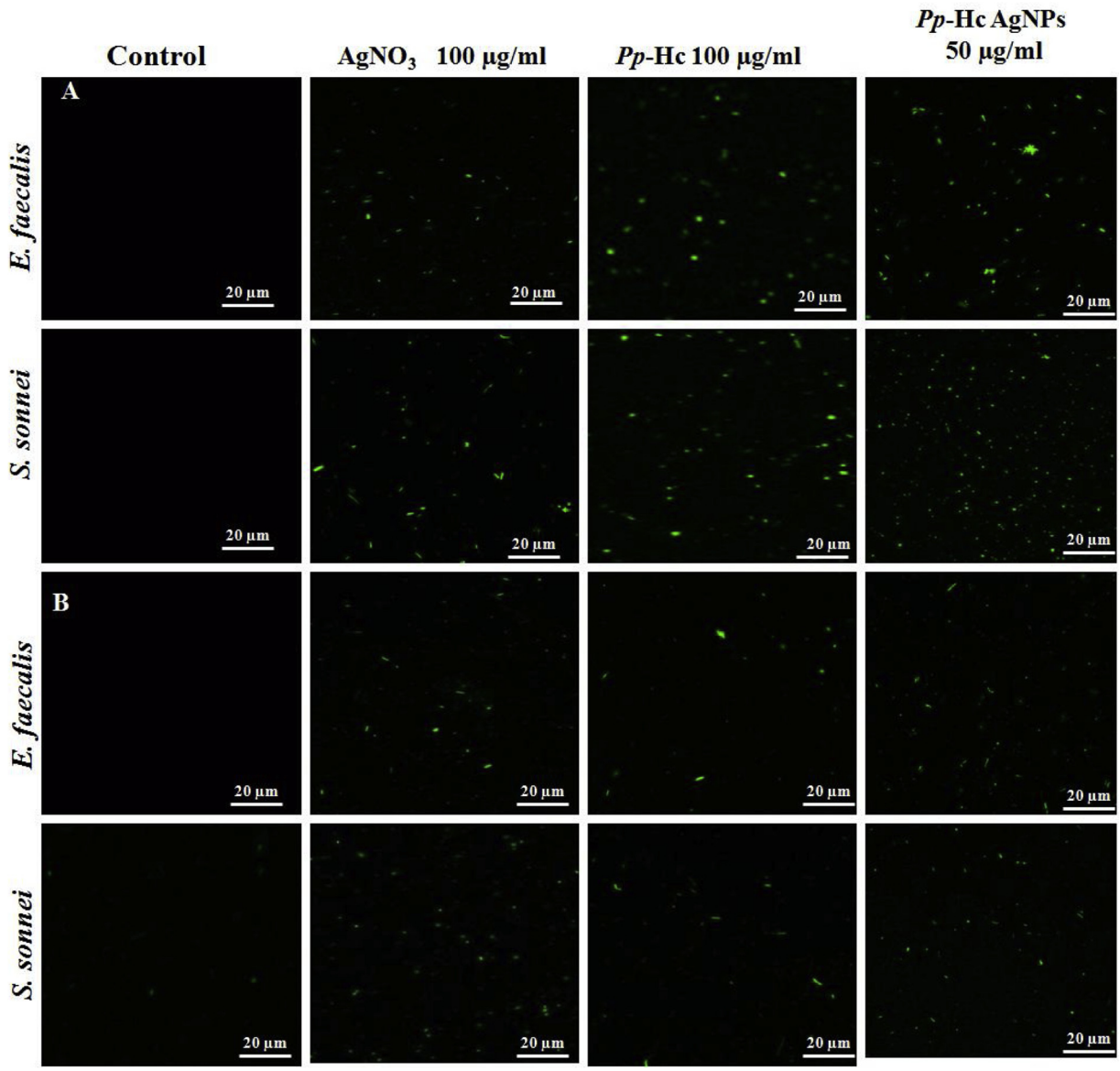

Fig. 5. Detection of bacterial intracellular ROS generation (A) and protein leakage (B) in the cells of *E. faecalis and S. sonnei* treated with $AgNO_3$, *Pp*-Hc and *Pp*-Hc AgNPs. Green fluorescence confirmed protein leakage in bacterial cells, while untreated cells show no fluorescence (For interpretation of the references to colour in this figure legend, the reader is referred to the web version of this article).

Hc and *Pp*-Hc AgNPs treated cell membranes were severely altered, the samples were stained with PI. PI can bind DNA or RNA, which results in fluorescence. Conversely, PI cannot cross the membrane and is expelled from possible cells [80]. Thus, bacterial cell injury is indicated by the release of nucleic acid from cells, whereas intracellular staining with PI can reveal dead cells. After treating the suspensions of *E. faecalis* and *S. sonnei* with $AgNO_3$, *Pp*-Hc and *Pp*-Hc AgNPs at 37 °C for 4 h followed by staining with PI, fluorescence assays showed that the permeability of treated bacteria was enhanced (Fig. 6a). The fluorescence clusters outside of cells showed that nucleic acids were released from the cells, in agreement with earlier studies [81,82].

3.9. Nanosilver-induced stress causes apoptosis of bacterial cells

A new key issue about nanoparticle toxicity in natural media is the capability to cause damage to the genetic material, as nanoparticles can cross the cell membranes to reach the cell nucleus. Only few studies have examined the genotoxicity of eco-friendly synthesized AgNPs – with special reference to those produced using crustacean-borne pure molecules - and their effects on DNA. Thus, additional research is needed. Small sized AgNPs may show superior reactivity, and thus high genotoxicity [83,84], but the particle size is not the only factor determining particle toxicity. Thus, the initiation of apoptosis was determined by examining the DNA fragmentation pattern. The $AgNO_3$, *Pp*-Hc and *Pp*-Hc AgNP-treated cells exhibits DNA strand streaks (lane IV–IX Fig. 6b). A similar trend was observed in earlier research, which showed that AgNPs considerably promoted either apoptosis or DNA fragmentation in bacterial cells [85,86].

3.10. Microscopic analysis of antibiofilm activity of purified Pp-Hc and Pp-Hc AgNPs

Biofilms are composed of a microbial consortium fixed in self-formed exopolymer matrices composed mainly of exopolysaccharides and serve as reservoirs for pathogenic organisms and are sources of disease outbreaks. Biofilms are observed in otitis media [87], otolaryngologic infections [88], osteomyelitis [89], bacterial endocarditis, cystic fibrosis [90], and non-healing wounds [91]. AgNPs have a special

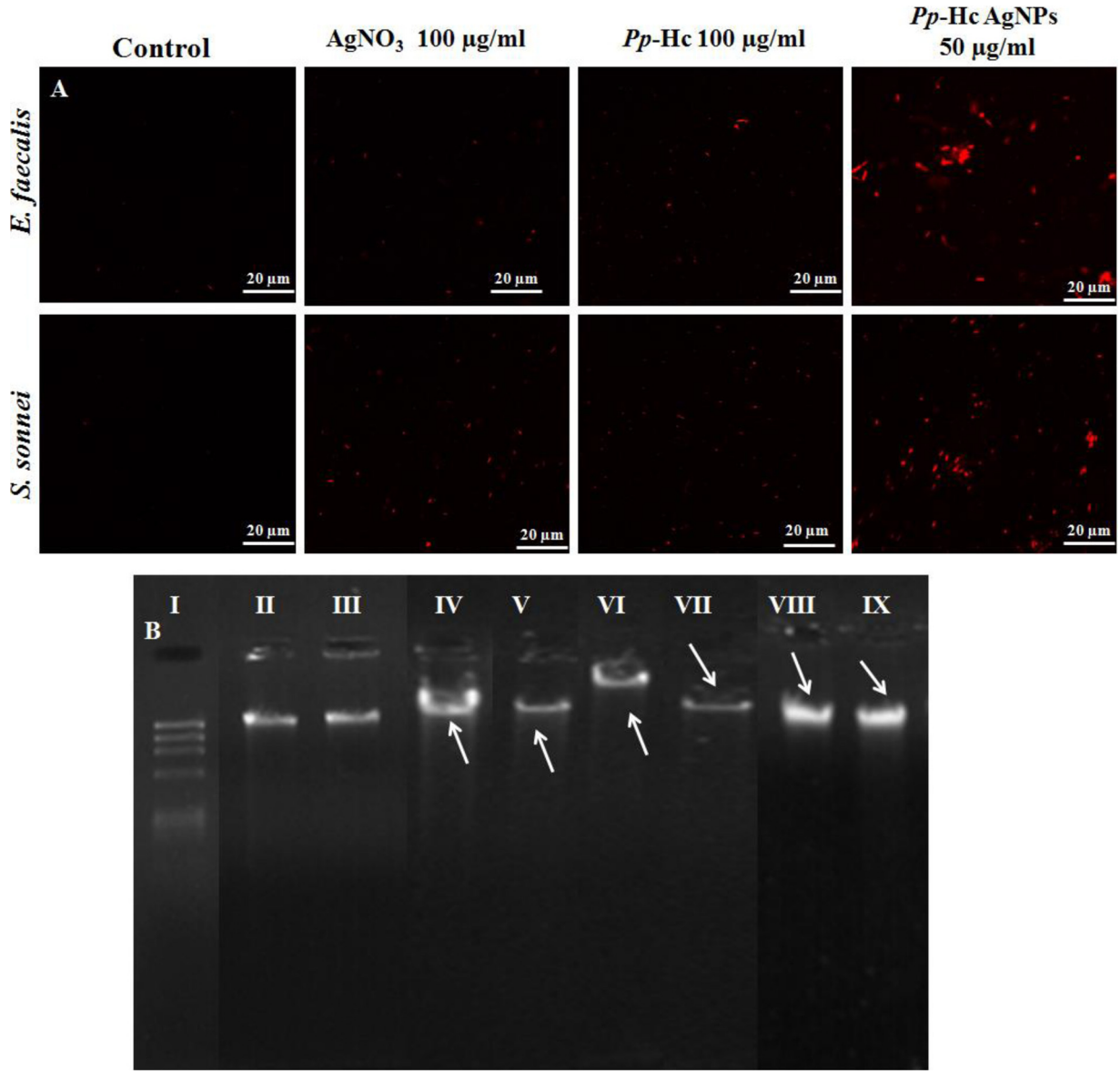

Fig. 6. Intracellular uptake of $AgNO_3$, *Pp*-Hc, and *Pp*-Hc-AgNPs in *E. faecalis* and *S. sonnei* bacteria examined using CLSM (A), detection of $AgNO_3$, *Pp*-Hc and *Pp*-Hc AgNPs induced apoptosis by DNA fragmentation (B). Analysis for bacterial DNA damage caused by $AgNO_3$, *Pp* Hc, and *Pp* Hc-AgNPs using 0.8% agarose gel electrophoresis. Lane I, 1 kB ladder. Lane II and III, control *E. faecalis* and *S. sonnei*. Lane IV to VI, $AgNO_3$, *Pp*-Hc and *Pp*-Hc AgNPs-treated *E. faecalis*. Lane VII to IX, $AgNO_3$, *Pp*-Hc and *Pp*-Hc AgNPs-treated *S. sonnei.* Arrow indicates the bacterial DNA damage.

capacity to disturb biofilm of numerous pathogenic bacteria. The $AgNO_3$, purified *Pp*-Hc and biosynthesized *Pp*-Hc AgNPs were tested for biofilm inhibition against *E. faecalis* and *S. sonnei*, which are known to form biofilms. Here, the surface morphology of *E. faecalis* and *S. sonnei* biofilm architecture and antibiofilm potency of $AgNO_3$, purified *Pp*-Hc and *Pp*-Hc AgNPs were evaluated by light microscopy, and CLSM analyses, and the purified *Pp*-Hc and *Pp*-Hc AgNPs were evaluated by SEM analyses. Results showed that $AgNO_3$, *Pp*-Hc and *Pp*-Hc AgNPs collapsed the biofilm architecture of the tested bacteria, resulting in the loosening and reduction of bacterial colonies (Figs. 7a,b and 8). Results revealed that the MIC concentration of *Pp*-Hc AgNPs (50 µg/mL) effectively reduced biofilm formation in tested bacteria compared to the purified *Pp*-Hc at a concentration of 100 µg/mL and $AgNO_3$ at a concentration of 100 µg/mL.

Additionally, the results of CLSM analysis revealed that the architecture of the biofilms was thicker and thinner over that of control (Fig. 8). The light, SEM, and CLSM microscopy showed that *Pp*-Hc AgNPs caused absolute dispersal of the biofilm architecture by loosening the micro-colonies in the treated sample. Our results concurred with those by Jayanthi et al. [47], who reported that lectin-coated AgNPs greatly reduced the *E. faecalis*, *B. pumilis*, *P. vulgaris*, and *P. aeruginosa* bacterial pathogens. Furthermore, Anjugam et al. [48] reported that *Pp* β-glucan-binding protein AgNPs efficiently killed bacterial colonies and biofilm-forming bacteria.

3.11. Dissolution of Ag^+

The dissolution of Ag^+ showed that the concentrations of releasing Ag^+ steadily improved by rising concentrations. The concentration of Ag^+ dissolved from 20 µg L^{-1} of NPs was 1.98 µg L^{-1}. At the highest concentration (100 µg L^{-1}) of NPs, 10 µg L^{-1} of soluble Ag^+ was detected in the present study (Fig. 9). Similarly, Vijayakumar et al. [92] reported that the highest concentration of NPs was 50 µg L^{-1} of SA – AgNPs showed 7.98 µg L^{-1} of soluble Ag^+ ions and Kim et al. [93] reported that 10 µg L^{-1} of citrate coated AgNPs (c-AgNPs) showed 4.86 µg/g dry weight of dissolved Ag^+ in the test

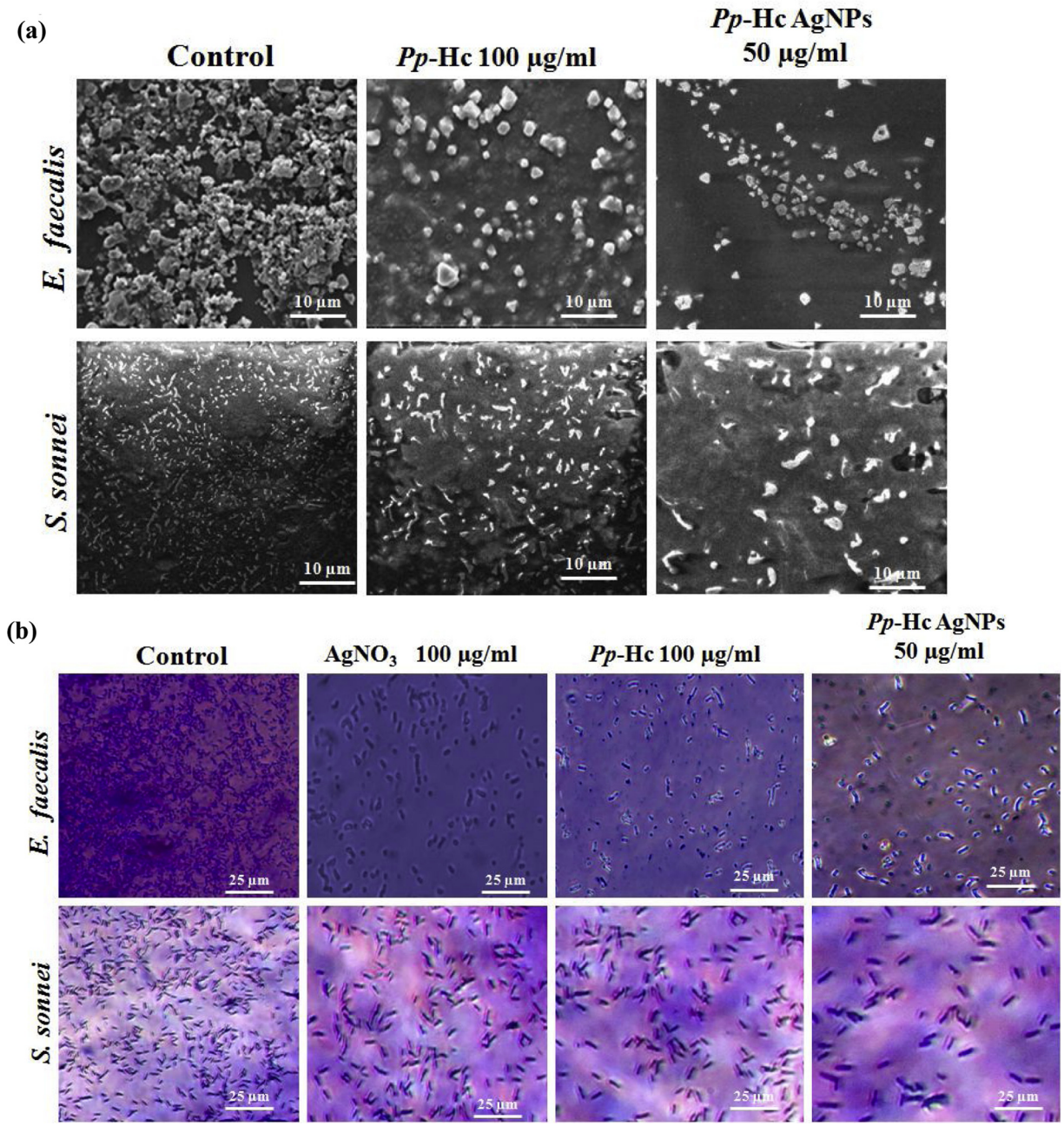

Fig. 7. SEM of *E. faecalis* and *S. sonnei* bacterial biofilms treated with *Pp*-Hc and *Pp*-Hc AgNPs, showing dispersed biofilm architecture (a) Antibiofilm activity of $AgNO_3$, *Pp*-Hc and *Pp*-Hc AgNPs visualized by light microscopy(b).

solution.

4. Conclusions

In this study, purified crab-borne hemocyanin was used for the rapid and effective synthesis of AgNPs by bio-reduction of aqueous Ag^+ ions. Interestingly, *Pp*-Hc AgNPs are promising antibacterial therapeutic agents against *E. faecalis* and *S. sonnei*. These *Pp*-Hc AgNPs exert toxicity towards bacteria by destroying the cell walls, undermining the cell membranes, and releasing the cellular contents such as nucleic acids and proteins. Furthermore, *Pp*-Hc AgNPs can efficiently prevent biofilm formation and rapidly kill bacteria at a rather low MIC. Thus, these *Pp*-Hc AgNPs are promising antibacterial materials for forthcoming biomedical purposes.

Conflict of interest

We wish to confirm that there are no known conflicts of interest associated with this publication.

Acknowledgements

The authors are grateful to the Council of Scientific and Industrial Research (CSIR), New Delhi, India for the financial assistance Rendered [Ref: 9/688 (0030)/18 EMR - I].The author thank to the RUSA phase 2.0 grant [Ref: 24-51/2014-U,Policy] TN Multi-Gen, Deptment of Edn Government of India. The authors extend their appreciation to the Deanship of Scientific Research at King Saud University for funding this work through research group No. RG-1438-091. The authors thank the Deanshipof Scientific Research and RSSU at King Saud University for

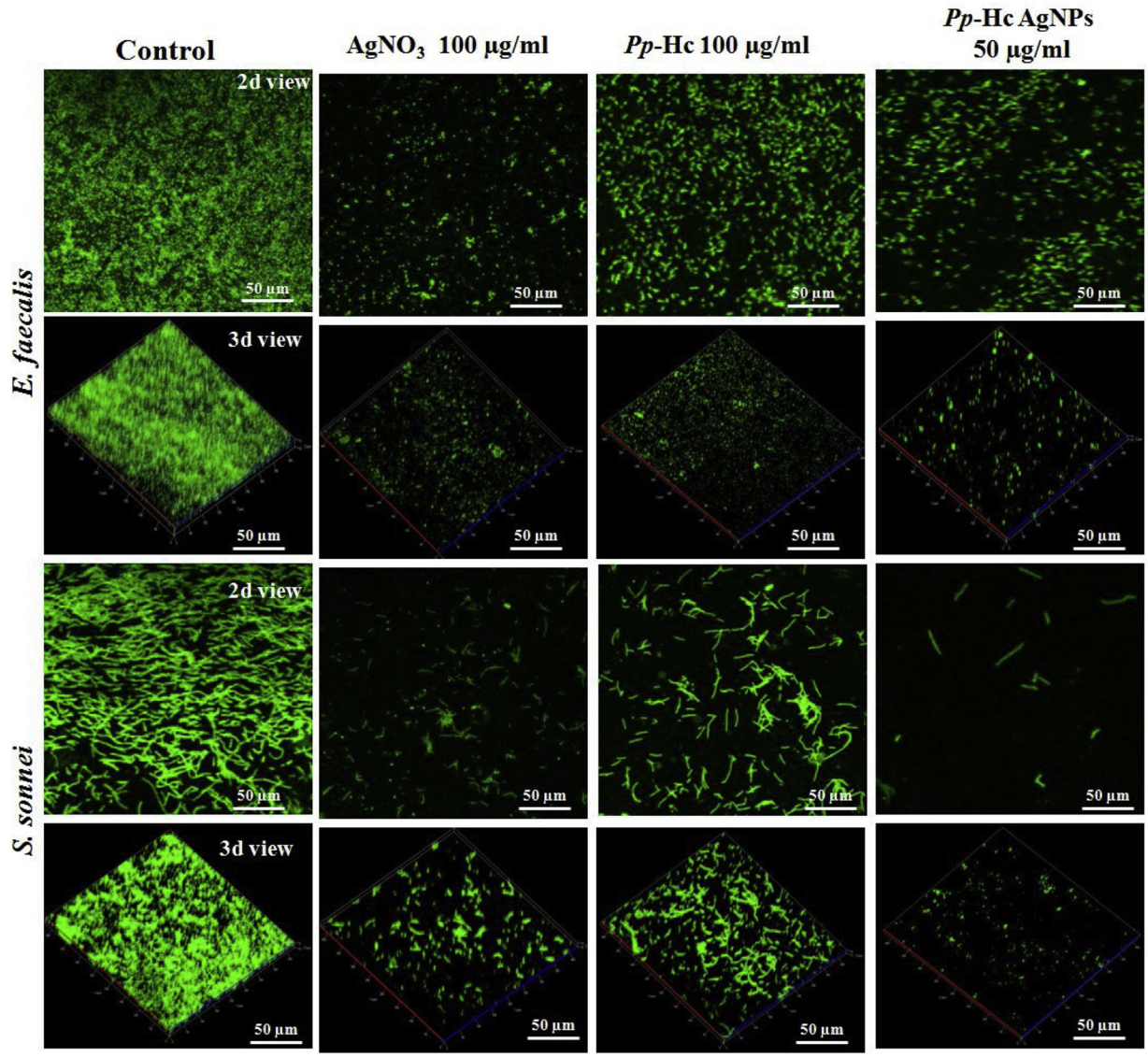

Fig. 8. CLSM image of bacterial biofilms grown in the presence or absence of $AgNO_3$, *Pp*-Hc and *Pp*-Hc AgNPs.

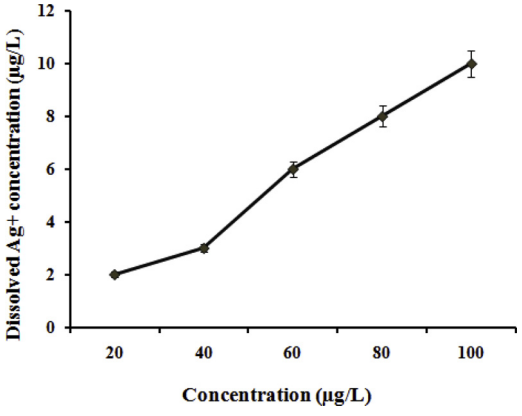

Fig. 9. Image of dissolved of Ag + from *Pp*-Hc AgNPs at different concentrations.

their technical support.

References

[1] H.C. Neu, The crisis in antibiotic resistance, Science 257 (1992) 1064–1073.
[2] D.I. Andersson, D. Hughes, Persistence of antibiotic resistance in bacterial populations, FEMS, Microbiol. Rev. 35 (2011) 901–911.
[3] D.I. Andersson, D. Hughes, Antibiotic resistance and its cost: is it possible to reverse resistance? Nat. Rev. Microbiol. 8 (2010) 260–271.
[4] G. Cheng, M. Dai, S. Ahmed, H. Hao, X. Wang, Z. Yuan, Antimicrobial drugs in fighting against antimicrobial resistance, Front. Microbiol. 7 (2016) 470.
[5] J.M. Muntia, C.A. Arias, Mechanisms of antibiotic resistance, Microbial. Spectr. 4 (2016) 10.
[6] K. Mijnendonckx, N. Leys, J. Mahillon, S. Silver, R. Van Houdt, Antimicrobial silver: uses, toxicity and potential for resistance, Biometals 26 (2013) 609–621.
[7] L.J. Shallcross, S.J. Howard, T. Fowler, S.C.D. Philos, Tackling the threat of antimicrobial resistance: from policy to sustainable action, Trans. R Soc. Lond. B Biol. Sci. 370 (2015) 20140082.
[8] H.J. Klasen, Historical review of the use of silver in the treatment of burns. I. Early uses, Burns 26 (2000) 117–130.
[9] J.W. Richard, B.A. Spencer, L.F. McCoy, E. Carina, J. Washington, P. Edgar, J. Rosenblatt, R. Goodheart, Acticoat versus silverlon: the truth, J. Burns. Surg. Wound. Care 1 (2002) 11–20.
[10] J.J. Castellano, S.M. Shafii, F. Ko, G. Donate, T.E. Wright, R.J. Mannari, Comparative evaluation of silver-containing antimicrobial dressings and drugs, Int. Wound J. 4 (2007) 114–122.
[11] M. Ramasamy, J. Lee, Recent nanotechnology approaches for prevention and treatment of biofilm-associated infections on medical devices, Bio. Med. Res. Int.

2016 (2016) 17.
[12] P.J.A. Borm, D. Robbins, S. Haubold, T. Kuhlbusch, H. Fissan, K. Donaldson, R. Schins, V. Stone, W. Kreyling, J. Lademann, J. Krutmann, D. Warheit, E. Oberdorster, The potential risks of nanomaterials: a review carried out for ECETOC, Part. Fibre Toxicol. 3 (2006) 11.
[13] G. Benelli, Green synthesized nanoparticles in the fight against mosquito-borne diseases and cancer - a brief review, Enzyme. Microbial. Technol. 95 (2016) 58–68.
[14] K. Gopinath, S. Kumaraguru, K. Bhakyaraj, S. Mohan, K.S. Venkatesh, M. Esakkirajan, P.R. Kaleeswarran, S.A. Naiyf, S. Kadaikunnan, M. Govindarajan, G. Benelli, A. Arumugam, Green synthesis of silver, gold and silver/gold bimetallic nanoparticles using the *Gloriosa superba* leaf extract and their antibacterial and antibiofilm activities, Microb. Pathogen 101 (2016) 1–11.
[15] W.H. De Jong, P.J.A. Borm, Drug delivery and nanoparticles: applications and hazards, Int. J. Nanomedicine 3 (2008) 133–149.
[16] M. Abinaya, B. Vaseeharan, M. Divya, A. Sharmili, M. Govindarajan, N.S. Alharbi, S. Kadaikunnan, J.M. Khaled, G. Benelli, Bacterial exopolysaccharide (EPS)-coated ZnO nanoparticles showed high antibiofilm activity and larvicidal toxicity against malaria and Zika virus vectors, J. Trace Elem. Med. Biol. 45 (2018) 93–103.
[17] S.M. Dizaj, A. Mennati, S. Jafari, K. Khezri, K. Adibkia, Antimicrobial activity of carbon-based nanoparticles, Adv. Pharm. Bull. 5 (2015) 19–23.
[18] M. Divya, B. Vaseeharan, M. Abinanya, S. Vijayakumar, M. Govindarajan, N.S. Alharbi, S. Kadaikunnan, J.M. Khaled, G. Benelli, Biopolymer gelatin-coated zinc oxide nanoparticles showed high antibacterial, antibiofilm and anti-angiogenic activity, J. Photochem. Photobiol. B 178 (2018) 211–218.
[19] R. Thaya, B. Vaseeharan, J. Sivakamavalli, A. Iswarya, M. Govindarajan, N.S. Alharbi, S. Kadaikunnan, M.N. Al-anbr, J.M. Khaled, G. Benelli, Synthesis of chitosan-alginate microspheres with high antimicrobial and antibiofilm activity against multi-drug resistant microbial pathogen, Microb. Pathogen. 114 (2018) 17–24.
[20] T. Hanemann, D.V. Szabó, Polymer-nanoparticle composites: from synthesis to modern applications, Materials 3 (2010) 3468–3517.
[21] E. Hoseinzadeh, P. Makhdoumi, P. Taha, H. Hossini, J. Stelling, M.A. Kamal, G.M. Ashraf, A review on nano-antimicrobials: metal nanoparticles, methods and mechanisms, Curr. Drug Metab. 18 (2017) 120–128.
[22] M. Govindarajan, S.L. Hoti, M. Rajeswary, G. Benelli, One-step synthesis of polydispersed silver nanocrystals using *Malva sylvestris*: an eco-friendly mosquito larvicide with negligible impact on non-target aquatic organisms, Parasitol. Res. 115 (2016) 2685–2695.
[23] B. Banumathi, B. Vaseeharan, B. Malaikozhundan, P. Ramasamy, M. Govindarajan, N.S. Alharbi, S. Kadaikunnan, A. Canale, G. Benelli, Green larvicides against blowflies, *Lucilia sericata* (Diptera, Calliphoridae): screening of seven plants used in Indian ethno-veterinary medicine and production of green-coated zinc oxide nanoparticles, Physiol. Mol. Plant Pathol. 101 (2018) 214–218.
[24] S.A. Alyahya, M. Govindarajan, N.S. Alharbi, S. Kadaikunnan, J.M. Khaled, B. Vaseeharan, R. Ishwarya, M. Yazhiniprabha, G. Benelli, Swift fabrication of Ag nanostructures using a colloidal solution of *Holostemma ada-kodien* (Apocynaceae) – antibiofilm potential, insecticidal activity against mosquitoes and non-target impact on water bugs, J. Photochem. Photobiol. B 181 (2018) 70–79.
[25] M. Govindarajan, M. Rajeswary, U. Muthukumaran, S.L. Hoti, H.F. Khater, G. Benelli, Single-step biosynthesis and characterization of silver nanoparticles using*Zornia diphylla* leaves: A potent eco-friendly tool against malaria and arbovirus vectors, J. Photochem. Photobiol. B 161 (2016) 482–489.
[26] X. Zhu, A.F. Radovic Moreno, J. Wu, R. Langer, J. Shi, Nanomedicine in the management of microbial infection – overview and perspectives, Nano Today 9 (2014) 478–498.
[27] G. Benelli, Plant-borne compounds and nanoparticles: challenges for medicine, parasitology and entomology, Environ. Sci. Pollut. Res. 25 (2018) 10149–10150.
[28] N. Beyth, Y. Houri-Haddad, A. Domb, W. Khan, R. Hazan, Alternative antimicrobial approach: nano-antimicrobial materials, Evid. Based Complement. Alternat.Med. 2015 (2015) 16.
[29] C. Marambio-Jones, E.M.V. Hoek, A review of the antibacterial effects of silver nanomaterials and potential implications for human health and the environment, J. Nanopart. Res. 12 (2010) 1531–1551.
[30] J.K. Patra, K.H. Baek, Green nanobiotechnology: factors affecting synthesis and characterization techniques, J. Nanomater. 2014 (2014) 12.
[31] R. Moosavi, S. Ramanathan, Y.Y. Lee, K.C. Siew Ling, A. Afkhami, G. Archunan, P. Padmanabhan, B. Gulyas, M. Kakran, S. Subramanian, T. Selvan, Synthesis of antibacterial and magnetic nanocomposites by decorating graphene oxide surface with metal nanoparticles, RSC Adv. 5 (2015) 76442–76450.
[32] J.S. Kim, E. Kuk, K.N. Yu, J. Kim, S.J. Park, H.L. Lee, S.H. Kim, Y.K. Park, M.S. Yong, C.Y. Hwang, Y.K. Kim, Y.S. Lee, D.H. Jeong, M.H. Cho, Antimicrobial effects of silver nanoparticles, Nanomedicine 3 (2007) 95–101.
[33] M. Raffi, F. Hussain, T.M. Bhatti, J.I. Akhter, A. Hameed, M.M. Hasan, Antibacterial characterization of silver nanoparticles against *E. coli* ATCC-15224, J. Mater. Sci. Technol. 24 (2008) 192–196.
[34] R. Sanghi, P. Verma, Biomimetic synthesis and characterisation of protein capped silver nanoparticles, Bioresour. Technol. 100 (2009) 501–504.
[35] X.F. Zhang, Z.G. Liu, W. Shen, S. Gurunathan, Silver nanoparticles: synthesis, characterization, properties, applications, and therapeutic approaches, Int. J. Mol. Sci 17 (2016) 1534.
[36] G. Benelli, F. Maggi, D. Romano, C. Stefanini, B. Vaseeharan, S. Kumar, A. Higuchi, A.A. Alarfaj, H. Mehlhorn, A. Canale, Nanoparticles as effective acaricides against ticks – a review, Ticks. Tick-Borne. Dis. 8 (2017) 821–826.
[37] N. Beyth, Y. Houri-Haddad, A. Domb, W. Khan, R. Hazan, Alternative antimicrobial approach: nano-antimicrobial materials, Evid. Based Complement. Alternat. Med. 2015 (2015) 16.
[38] C. Aarthi, M. Govindarajan, P. Rajaraman, N.S. Alharbi, S. Kadaikunnan, J.M. Khaled, R.A. Mothana, N.A. Siddiqui, G. Benelli, Eco-friendly and cost effective Ag nanocrystals fabricated using the leaf extract of *Habenaria plantaginea*: toxicity on six mosquito vectors and four non-target species, Environ. Sci. Pollut. Res. 25 (2018) 10317–10327.
[39] M. Govindarajan, H.F. Khater, C. Panneerselvam, G. Benelli, One-pot fabrication of silver nanocrystals using *Nicandra physalodes*: a novel route for mosquito vector control with moderate toxicity on non-target water bugs, Res. Vet. Sci 107 (2016) 95–101.
[40] P. Kuppusamy, M.M. Yusoff, G.P. Maniam, N. Govindan, Biosynthesis of metallic nanoparticles using plant derivatives and their new avenues in pharmacological applications – an updated report, Saudi Pharm. J. 24 (2016) 473–484.
[41] R.G. Saratale, H.S. Shin, G. Kumar, G.S. Ghodake, Y.Y. Jiang, G. Benelli, D.S. Kim, G.D. Saratale, Exploiting fruit byproducts for eco-friendly nanosynthesis: *citrus clementina* peel extract mediated fabrication of silver nanoparticles with high efficacy against microbial pathogens and rat glial tumor C6 cells, Environ. Sci. Pollut. Res. 25 (2018) 10250–10263.
[42] K.S. Siddiqi, A. Husen, R.A.K. Rao, A review on biosynthesis of silver nanoparticles and their biocidal properties, Nanobiotechnology 16 (2018) 14.
[43] D.M. Eby, N.M. Schaeublin, N.M. Farrington x, S.M. Hussain, G.R. Johnson, Lysozyme catalyzes the formation of antimicrobial silver nanoparticles, ACS Nano 3 (2009) 984–994.
[44] S. Sharma, S. Mandani, T.K. Sarma, Biogenic growth of alloys and core-shell nanostructures using urease as a nanoreactor at ambient condition, Sci. Rep. 3 (2013) 1–8.
[45] A.T. Aziz Ali, M. Alshehri, C. Panneerselvam, K. Murugan, S. Trivedi, J.A. Mahyoub, M.M. Hassan, F. Maggi, S. Sut, S. Dall'Acqua, A. Canale, G. Benelli, The desert wormwood (*Artemisia herba-alba*) – from Arabian folk medicine to a source of green and effective nanoinsecticides against mosquito vectors, J. Photochem. Photobiol. B 180 (2018) 225–234.
[46] R. Ishwarya, B. Vaseeharan, R. Jayakumar, V. Ramasubramanian, M. Govindarajan, N.S. Alharbi, S. Kadaikunnan, J.M. Khaled, G. Benelli, Bio-mining drugs from the sea: high antibiofilm properties of haemocyanin purified from the haemolymph of flower crab*Portunus pelagicus* (L.) (Decapoda: Portunidae), Aquaculture 489 (2018) 130–140.
[47] S. Jayanthi, S. Shanthi, B. Vaseeharan, N. Gopi, M. Govindarajan, N.S. Alharbi, S. Kadaikunnan, J.M. Khaled, B. Benelli, Growth inhibition and antibiofilm potential of Ag nanoparticles coated with lectin, an invertebrate immune molecule, J. Photochem. Photobiol. B 170 (2017) 208–216.
[48] M. Anjugam, B. Vaseeharan, A. Iswarya, M. Divya, N.M. Prabhu, K. Sankaranarayanan, Biological synthesis of silver nanoparticles using β-1, 3 glucan binding protein and their antibacterial, antibiofilm and cytotoxic potential, Microb. Pathogen 115 (2017) 31–40.
[49] A. Iswarya, B. Vaseeharan, M. Anjugam, B. Ashokkumar, M. Govindarajan, N.S. Alharbi, S. Kadaikunnan, J.M. Khaled, G. Benelli, Multipurpose efficacy of ZnO nanoparticles coated by the crustacean immune molecule β-1, 3-glucan binding protein: toxicity on HepG2 liver cancer cells and bacterial pathogens, Colloids Surf. B Biointerfaces 158 (2017) 257–269.
[50] S. Chowdhury, A. Basu, S. Kundu, Green synthesis of protein capped silver nanoparticles from phytopathogenic fungus *Macrophomina phaseolina* (Tassi) Goid with antimicrobial properties against multidrug-resistant bacteria, Nanoscale Res. Lett. 9 (2014) 1-1.
[51] N. Jain, A. Bhargava, M. Rathi, V. Dilip, J. Panwar, Removal of protein capping enhances the antibacterial efficiency of biosynthesized silver nanoparticles, PLoS One 10 (2015) 0134337.
[52] R. Ishwarya, B. Vaseeharan, A. Iswarya, S. Karthikeyan, Haemolytic and antibiofilm properties of haemocyanin purified from the haemolymph of Indian white shrimp Fenneropenaeus indicus, Fish Shellfish Immunol. 59 (2016) 447–455.
[53] J. Luo, J. Kong, B.Y. Dong, H. Huang, K. Wang, L.H. Wu, Y.Q. Chen, Baicalein attenuates the quorum sensing-controlled virulence factors of *Pseudomonas aeruginosa* and relieves the inflammatory response in *P aeruginosa*-infected macrophages by down regulating the MAPK and NFkB signal-transduction pathways, Drug Des. Devel. Ther. 10 (2016) 183–203.
[54] A. Hochman, I. Goldberg, Purification and characterization of a catalase-peroxidase and a typical catalase from the bacterium Klebsiella pneumoniae, Biochem. Biophys. Acta 1077 (1991) 299–307.
[55] S. Arora, J. Jain, J.M. Rajwade, K.M. Paknikar, Cellular responses induced by silver nanoparticles: in vitro studies, Toxicol. Lett. 79 (2008) 93–100.
[56] J.A. Buege, S.D. Aust, Microsomal lipid peroxidation, in: S. Fleischer, L. Packer (Eds.), Methods in Enzymology, 52 Academic Press, New York, 1978, pp. 303–310.
[57] V. Gopinath, S. Priyadarshini, M.F. Loke, J. Arunkumar, E. Marsili, D. MubarakAli, P. Velusamy, J. Vadivelu, Biogenic synthesis, characterization of antibacterial silver nanoparticles and its cell cytotoxicity, Arab. J. Chem. 10 (2015) 1107–1117.
[58] K.D. Datkhile, P.P. Durgawale, P.P. Patil, Biogenic silver nanoparticles are equally cytotoxic as chemically synthesized silver nanoparticles, Biomed. Pharmacol. J. 10 (2017) 337–344.
[59] J. Alves, V.V. Marques, L.F.P. Pereira, E.Y. Hirooka, T.C.R.M. Oliveira, Multiplex PCR for the detection of *Campylobacter* spp. and *Salmonella* spp. in chicken meat, J. Food. Saf. 32 (2012) 345–350.
[60] S. Chowdhuri, A. Basu, S. Kundu, Green synthesis of protein capped silver nanoparticles from phytopathogenic fungus *Macrophomina phaseolina* (Tassi) Goid with antimicrobial properties against multidrug-resistant bacteria, Nanoscale Res. Lett. 9 (2014) 365.
[61] S.M. Ouda, Antifungal activity of silver and copper nanoparticles on two plant pathogens, *Alternaria alternata* and *Botrytis cinerea*, Res. J. Microbiol. 9 (2014) 34–42.

[62] A.V. Delgado, F. González-Caballero, R.J. Hunter, L.K. Koopal, J. Lyklema, Measurement and interpretation of electrokinetic phenomena, Pure Appl. Chem. 77 (2005) 1753–1805.
[63] F.N. Fu, D.B.D. Olieveira, W.R. Trumble, H.K. Sarkar, B.R. Singh, Secondary structure estimation of proteins using the Amide III region of Fourier transform infrared spectroscopy: application to analyze calcium-binding induced structural changes in calsequestrin, Appl. Spectrosc. 48 (1994) 1432–1441.
[64] F.V. Germar, A. Galan, O. Llorca, J.L. Carrascosa, J.M. Valpuesta, W. Mantele, A. Muga, Conformational changes generated in GroEL during ATP hydrolysis as seen by time-resolved infrared spectroscopy, J. Biol. Chem. 274 (1999) 5508–5513.
[65] J. Corbin, N. Methot, H.H. Wang, J.E. Baenziger, M.P. Blanton, Secondary structure analysis of individual transmembrane segments of the nicotinic acetylcholine receptor by circular dichroism and Fourier transform infrared spectroscopy, J. Biol. Chem. 273 (1998) 771.
[66] D. Ballottin, S. Fulaz, M.L. Souza, P. Corio, A.G. Rodrigues, A.O. Souza, P.M. Gaspari, A.F. Gomes, F. Gozzo, L. Tasic, Elucidating protein involvement in the stabilization of the biogenic silver nanoparticles, Nanoscale Res. Lett. 11 (2016) 313.
[67] M. Rai, A. Yadav, A. Gade, Silver nanoparticles as a new generation of antimicrobials, Biotechnol. Adv. 27 (2009) 76–83.
[68] R. Foldbjerg, D.A. Dang, H. Autrup, Cytotoxicity and genotoxicity of silver nanoparticles in the human lung cancer cell line, A549, Arch. Toxicol. 85 (2011) 743–750.
[69] S. Kim, J.E. Choi, J. Cho, K.H. Chung, K. Park, J. Yi, D.Y. Ryu, Oxidative stress-dependent toxicity of silver nanoparticles in human hepatoma cells, Toxicology 23 (2009) 1076–1084.
[70] J.R. Morones, J.L. Elechiguerra, A. Camacho, K. Holt, J.B. Kouri, J.T. Ramírez, M.J. Yacaman, The bactericidal effect of silver nanoparticles, Nanotechnology 16 (2005) 2346–2353.
[71] R. Lima, A.B. Seabra, N. Durán, Silver nanoparticles: a brief review of cytotoxicity and genotoxicity of chemically and biogenically synthesized nanoparticles, J. Appl. Toxicol. 32 (2012) 867–879.
[72] C.M. Sayes, A.M. Gobin, K.D. Ausman, J. Mendez, J.L. West, V.L. Colvin, Nano-C60 cytotoxicity is due to lipid peroxidation, Biomaterials 26 (2005) 7587–7595.
[73] E.E. Farmer, M.J. Mueller, ROS-mediated lipid peroxidation and RES-activated signaling, Annu. Rev. Plant Biol. 64 (2013) 429–450.
[74] C.N. Lok, C.M. Ho, R. Chen, Q.Y. He, W.Y. Yu, H. Sun, P.K. Tam, J.F. Chiu, C.M. Che, Proteomic analysis of the mode of antibacterial action of silver nanoparticles, J. Proteome Res. 5 (2006) 916–924.
[75] P. Wu, J.A. Imlay, J.K. Shang, Mechanism of Escherichia coli inactivation on palladium-modified nitrogen-doped titanium dioxide, Biomaterials 31 (2010) 7526–7533.
[76] R. Vazquez Munoz, B. Borrego, K.J. Moreno, M.G. Garcia, J.D.M. Morales, N. Bogdanchikova, A.H. Saqero, Toxicity of silver nanoparticles in biological systems: does the complexity of biological systems matter? Toxicol. Lett. 276 (2017) 11–20.
[77] P.C. Naha, H.J. Byrne, Generation of intracellular reactive oxygen species and genotoxicity effect to exposure of nanosized polyamidoamine (PAMAM) dendrimers in PLHC-1 cells in vitro, Aquat. Toxicol. 132–133 (2013) 61–72.
[78] S. Dwivedi, R. Wahab, F. Khan, Y.K. Mishra, J. Musarrat, A.A. Al-Khedhairy, Reactiveoxygen species mediated bacterial biofilm inhibition via zinc oxide nanoparticles and their statistical determination, PLoS One 9 (2014) 111289.
[79] P.P. Fu, Q. Xia, H.M. Hwang, P.C. Ray, H. Yu, Mechanisms of nanotoxicity: generation of reactive oxygen species, J. Food Drug Anal. 22 (2014) 64–75.
[80] Y.Y. Zhao, Y. Tian, Y. Cui, W.W. Liu, W.S. Ma, X.Y. Jiang, Small molecule-capped gold nanoparticles as potent antibacterial agents that target Gram-negative bacteria, J. Am. Chem. Soc. 132 (2010) 12349–12356.
[81] O. Choi, K.K. Deng, N.J. Kim, L. Ross, R.Y. Surampalli, Z. Hu, The inhibitory effects of silver nanoparticles, silver ions, and silver chloride colloids on microbial growth, Water Res. 42 (2008) 3066–3074.
[82] A. Travan, C. Pelillo, I. Donati, E. Marsich, M. Benincasa, T. Scarpa, Non-cytotoxic silver nanoparticle- polysaccharide nanocomposites with antimicrobial activity, Biomacromolecules 10 (2009) 1429–1435.
[83] C.G. Ordzhonikidze, L.K. Ramaiyya, E.M. Egorova, A.V. Rubanovich, Genotoxic effects of silver nanoparticles on mice in vivo, Acta Naturae 3 (2009) 99–101.
[84] J.S. Kim, J.H. Sung, J.H. Ji, K.S. Song, J.H. Lee, C.S. Kang, I.J. Yu, In vivo genotoxicity of silver nanoparticles after 90-day silver nanoparticle inhalation exposure, Saf. Health Work 2 (2011) 34–38.
[85] P. Velusamy, J. Dasa, R. Pachaiappana, B. Vaseeharan, K. Pandian, Greener approach for synthesis of antibacterial silver nanoparticles using aqueous solution of neem gum (*Azadirachta indica* L.), Ind. Crop. Prod. 66 (2015) 103–109.
[86] B. Rout, C.H. Liu, W.C. Wu, Photosensitizer in lipid nanoparticles a: nano-scaled approach to antibacterial function, Sci. Rep. 7 (2017) 7892.
[87] L.O. Bakaletz, Bacterial biofilms in otitis media: evidence and relevance, Pediatr. Infect. Dis. J. 26 (2007) 17–19.
[88] J.C. Post, N.L. Hiller, L. Nistico, P. Stoodley, G.D. Ehrlich, The role of biofilms in otolaryngologic infections, Curr. Opin. Otolaryngol. Head Neck Surg. 15 (2007) 347–351.
[89] R.A. Brady, J.G. Leid, J.H. Calhoun, J.W. Costerton, M.E. Shirtliff, Osteomyelitis and the role of biofilms in chronic infection, FEMS Immunol. Med. Microbiol. 52 (2008) 13–22.
[90] N. Hoiby, Understanding bacterial biofilms in patients with cystic fibrosis: current and innovative approaches to potential therapies, J. Cyst. Fibros. 1 (2002) 249–254.
[91] G.A. James, E. Swogger, R. Wolcott, E. Pulcini, P. Secor, J. Sestrich, J.W. Costerton, P.S. Stewart, Biofilms in chronic wounds, Wound Repair Regen. 16 (2008) 37–44.
[92] S. Vijaya kumar, B. Malaikozhundan, P. Ramasamy, B. Vaseeharan, Assessment of biopolymer stabilized silver nanoparticles for their ecotoxicity on *Ceriodaphnia cornuta* and antibiofilm activity, J. Environ. Chem. Eng. 4 (2016) 2076–2083.
[93] I. Kim, B.T. Lee, H.A. Kim, K.W. Kim, S.D. Kim, Y.S. Hwang, Citrate coated silver nanoparticles change heavy metal toxicities and bioaccumulation of *Daphnia magna*, Chemosphere 143 (2015) 99–105.